

Double-slit interference of biphotons generated in spontaneous parametric downconversion from a thick crystal

A F Abouraddy, B E A Saleh, A V Sergienko and M C Teich

Quantum Imaging Laboratory, Departments of Electrical & Computer Engineering and Physics, Boston University, 8 Saint Mary's Street, Boston, MA 02215, USA

E-mail: raddy@bu.edu

Received 4 July 2000, in final form 10 January 2001

Abstract

In this paper we investigate the fourth-order coherence of biphoton beams from spontaneous parametric downconversion resulting from a nonlinear crystal as exemplified in a double-slit interference configuration where the signal and idler beams both pass through the same double slits. We find that the angle of the crystal optical axis and the crystal length are important factors, along with the double-slit separation and system bandwidth, in determining the nature of the fourth-order interference pattern obtained behind the slits. Only careful planning of system parameters and understanding of the tuning curves of the downconversion will illuminate the obtained coincidence patterns.

Keywords: Quantum interference, spontaneous parametric downconversion, fourth-order coherence, quantum entanglement, double-slit interference

1. Introduction

Young's double-slit interference experiment is synonymous with the determination of the coherence properties of light. It has been used, classically, to determine the second-order coherence function by measuring the visibility of the fringes formed behind the double slit as the slit separation changes [1]. The development of nonclassical sources of light has helped envisage new double-slit interference experiments where both second- and fourth-order coherence properties are measured [2–5]. One such source is the light generated through the process of spontaneous parametric downconversion (SPDC). In this process a pump beam generates two highly correlated beams, called signal and idler beams, through a nonlinear interaction. Such twin beams are usually called entangled beams, and they have unusual and sometimes unintuitive properties compared to classical light sources. For example, the fourth-order coherence function (two-photon coincidence pattern) has an analogous form to that of the second-order coherence function of a partially coherent classical source [6]. Such behaviour can be investigated in double-slit configurations.

In one configuration the signal beam is sent through the double slit and then detected by a single-photon detector, whilst the idler beam is detected by another single-photon

detector, and the coincidence of detection at both detectors are registered while one of the detectors is scanned in the direction perpendicular to the expected classical second-order fringes [2]. Such an experiment yields coincidence fringes analogous to the familiar intensity fringes. In another configuration both signal and idler beams are sent through the double slit [3–5]. This is the case to be studied in this paper and is the case most resembling that of the classical case in experimental set-up. We will show that such a configuration yields a coincidence pattern that is highly sensitive to the source (crystal) characteristics, giving more degrees of freedom compared to the classical case.

2. Theory

In a recent paper [6] we studied in detail the duality between partial coherence and partial entanglement in the context of biphoton beams produced by SPDC. In that paper we developed a set of equations that can be used to calculate the fourth-order coherence function, which is a measure of coincidence of the photon pairs, comprising a biphoton, after they traverse an optical system. In this paper we briefly review the equations developed there and apply them to the case of double-slit interference.

Assume an optical pump beam (usually a collimated laser beam, hereinafter referred to as the ‘pump’ and denoted by p) impinges on a nonlinear crystal (NLC), normal to its surface. If the crystal has an appreciable second-order nonlinearity, the nonlinear interaction will lead to the pump photons spontaneously disintegrating into two photons known (for historical reasons) as the signal (s) and idler (i). The signal and idler photons are highly correlated in frequency and direction since their generation follows the rules of conservation of energy and momentum, $\omega_p = \omega_s + \omega_i$ and $\vec{k}_p = \vec{k}_s + \vec{k}_i$, respectively, also known as the phase matching conditions, where ω and \vec{k} represent angular frequency and momentum.

We next assume that the signal and idler beams traverse optical systems having classical optical impulse response functions $h_s(x_1, x; \omega_s)$ and $h_i(x_2, x; \omega_i)$, where the subscripts s and i again refer to signal and idler respectively, x_1 and x_2 are two points on the output observation plane, and x is a point on the input face of the crystal used to describe the impinging pump electric-field distribution, $E_p(x)$. We have shown that for a monochromatic pump, NLC of thickness ℓ , and spectral filters of bandwidth Ω , the coincidence rate at the output plane is given by [6, equation (4.14)]

$$C(x_1, x_2) = \int_{\Omega} |\tilde{\psi}(x_1, x_2; \omega_s)|^2 d\omega_s, \quad (1)$$

where $\tilde{\psi}(x_1, x_2; \omega_s)$ is a spectral probability amplitude given by

$$\tilde{\psi}(x_1, x_2; \omega_s) = \frac{1}{4\pi^2} \iint \Lambda(q_s, q_i; \omega_s) \times H_s(x_1, q_s; \omega_s) H_i(x_2, q_i; \omega_p - \omega_s) dq_s dq_i. \quad (2)$$

The quantity $H_s(x_1, q_s; \omega_s)$ is the Fourier transform of $h_s(x_1, x; \omega_s)$ with respect to the parameter x , and $H_i(x_2, q_i; \omega)$ is defined similarly; q_s and q_i are the transverse components of the signal and idler wavevectors, respectively, and the kernel $\Lambda(q_s, q_i; \omega_s)$ is related to the pump field distribution and the degree of phase-matching through the relation [6, equation (5.9)]

$$\Lambda(q_s, q_i; \omega_s) = \tilde{E}_p(q_s + q_i) \tilde{\zeta}(q_s, q_i; \omega_s). \quad (3)$$

Here $\tilde{E}_p(q)$ is the Fourier transform of the pump spatial distribution $E_p(x)$ and $\tilde{\zeta}(q_s, q_i; \omega_s)$ is a function that describes the degree of phase-matching between the signal and idler beams [6, equation (5.10)]:

$$\tilde{\zeta}(q_s, q_i; \omega_s) = \ell \text{sinc} \left[\frac{\ell}{2\pi} \left(\sqrt{\frac{\omega_p^2 n^2(\omega_p)}{c^2} - (q_s + q_i)^2} - \sqrt{\frac{\omega_s^2 n^2(\omega_s)}{c^2} - q_s^2} - \sqrt{\frac{(\omega_p - \omega_s)^2 n^2(\omega_p - \omega_s)}{c^2} - q_i^2} \right) \right]. \quad (4)$$

Through $\tilde{\zeta}(q_s, q_i; \omega_s)$ the effect of the length of the crystal ℓ and its physical characteristics: its indices of refraction at the pump, signal, and idler frequencies and polarizations, along with the angle of the optical axis of the anisotropic crystal with respect to the normal to the crystal surface (i.e. the optical axis

of the external optical system) is manifested. The sinc function gives us the probability amplitude of each pair of signal/idler frequencies having a certain pair of signal/idler directions.

The function $\tilde{\zeta}(q_s, q_i; \omega_s)$ assumes two limiting forms that are important in the sequel. The thin-crystal limit is obtained when ℓ is very small whereas the thick-crystal limit results when ℓ is very large. In the thin-crystal limit the sinc function of $\tilde{\zeta}(q_s, q_i; \omega_s)$ becomes almost constant over a wide range of frequencies and directions. The kernel $\Lambda(q_s, q_i; \omega_s)$ in (2) then becomes simply $\tilde{E}_p(q_s + q_i)$ and the physical characteristics of the crystal have little effect. In the thick-crystal limit the width of the sinc function becomes very small and tends towards a delta function. This means that each frequency is spread over a very narrow range of directions.

3. Tuning curves

As mentioned in the previous section, the function $\tilde{\zeta}(q_s, q_i; \omega_s)$ determines the nature of the relation between the frequencies of a signal/idler biphoton pair and the directions at which the signal and idler modes will be emitted [7]. For each signal mode frequency, there is a set of directions at which we expect it to be emitted with high probability (where the sinc function peaks). There will be low probability for this signal mode frequency to be emitted in all other directions (the tails of sinc function).

We calculated the tuning curves for three thicknesses (0.1, 1 and 10 mm) of a Beta-Barium Borate (BBO) crystal pumped at a wavelength of 325 nm (which corresponds to an ultraviolet line of a He–Cd laser) for type-I downconversion (signal and idler both have ordinary polarization with respect to the crystal optical axis, whilst the pump has extraordinary polarization). The calculations were performed for three orientations of the crystal with respect to the normal direction to the crystal surface (denoted by φ): 36.30° , 36.50° and 36.44° .

Figure 1 shows the resulting tuning curves of this BBO crystal with the above mentioned parameters. In all figures, the horizontal axes refer to the emitted frequencies normalized to the pump frequency, and the vertical axes refer to the angle at which the photons are emitted in radians, with respect to the normal to the surface of the crystal. The first column shows the results for $\varphi = 36.30^\circ$ as we proceed from a 0.1 to a 10 mm thick crystal. We clearly observe the decreasing level of uncertainty of the angles at which each frequency is being emitted from the crystal. The same observation is clear in the second and third columns. Another feature is the drastic change in the shape of the tuning curves with change in the crystal angle φ . For example, the first column shows that there is no emission at the degenerate frequency ($\omega_0 = \omega_p/2$). The collinear downconversion (i.e. the emission angle is 0) occurs with a non-degenerate pair. In the second column we have a noncollinear degenerate case. In the third column we have a collinear degenerate case. We shall show how this change in the shape of the tuning curves leads to different results in a double-slit interference configuration.

4. Double-slit configuration

We now turn to the interferometric configuration that is the principal purpose of this paper. Let us consider the signal

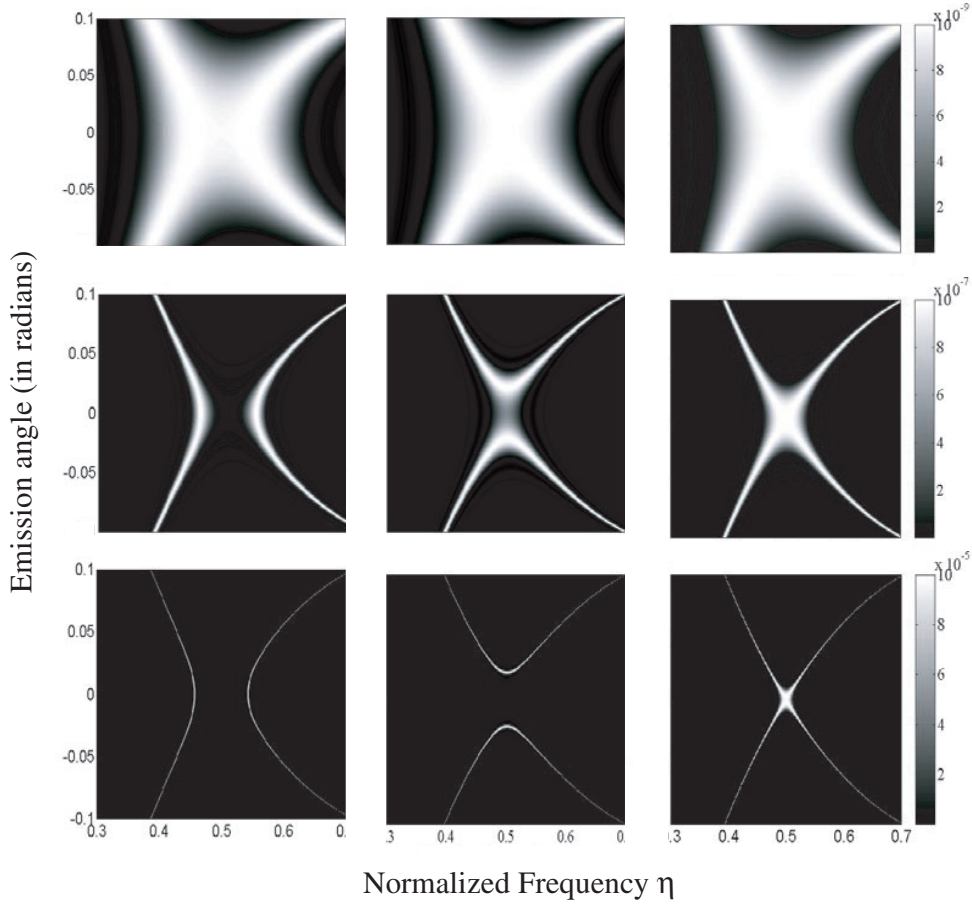


Figure 1. Tuning curves for type-I downconversion from a BBO crystal. Pump wavelength is 325 nm. Proceeding from top to bottom we change the crystal length from 0.1 to 1 mm and then 10 mm. In all figures, the horizontal axes refer to the emitted frequencies normalized to the pump frequency, and the vertical axes refer to the angle at which the photons are emitted in radians, with respect to the normal to the surface of the crystal. The first column corresponds to $\varphi = 36.30^\circ$, the second to $\varphi = 36.44^\circ$, and the third to $\varphi = 36.50^\circ$.

and idler photons traversing a $4f$ system (which serves as a generic linear shift-invariant system) as shown in figure 2. The aperture $t(x)$ in the Fourier plane is, in our case, a double slit, given by

$$t(x) = \text{rect}\left(\frac{x - a/2}{b}\right) + \text{rect}\left(\frac{x + a/2}{b}\right), \quad (5)$$

where the function $\text{rect}(x)$ is a uniform function of width unity, a is the distance between the centres of the slits, and b is the width of each slit. We shall define $p = b/a$ as the relative width of the slit with respect to the separation of the centres. In this case, the transfer functions of both the signal and idler are

$$H_s(x, q; \omega) = H_i(x, q; \omega) \propto e^{-ixq} t_s\left(\frac{cf}{\omega}q\right), \quad (6)$$

where $t_s(x) = t_i(x) = t(x)$. Assuming a pump width large in comparison to all the apertures in the system, $\tilde{E}_p(q)$ becomes approximately a delta function, which leads to a spectral probability amplitude

$$\begin{aligned} \tilde{\psi}(x_1, x_2; \omega_s) &\propto \int_{-\infty}^{\infty} dq_s e^{-q_s(x_1 - x_2)} \tilde{\zeta} \\ &\times (q_s, -q_s; \omega_s) t_s\left(\frac{cf}{\omega_s}q_s\right) t_i\left(\frac{cf}{\omega_p - \omega_s}q_s\right). \end{aligned} \quad (7)$$

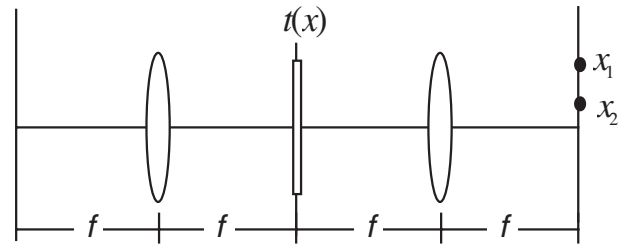


Figure 2. Schematic of the $4f$ system used in the calculations.

The coincidence rate is obtained by substituting this spectral probability amplitude into (1). The coincidence rate at the output plane is a function of only the separation of the two points under consideration, a direct result of assuming a large pump width.

We now introduce some normalized parameters to cast the previous equations into a simpler form. We define a normalized frequency $\eta = \omega_s/\omega_p$ and a normalized bandwidth $\rho = \Omega/\omega_p$ so that η will thus assume values of $(1 - \rho)/2$ to $(1 + \rho)/2$, with a maximum value of $\rho = 1$. We further define $\theta = a/f$, the angle subtended by the double slits at the crystal, and a characteristic distance $\Lambda = 2\lambda_p/\theta$, where λ_p is the pump

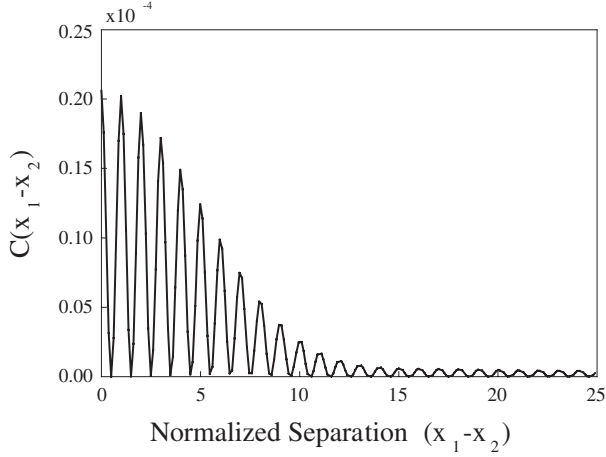


Figure 3. Coincidence rate as a function of normalized separation for $\varphi = 36.44^\circ$, $\ell = 0.1$ mm, $\theta = 0.03$, $p = 0.1$, $\rho = 0.05$.

wavelength. Equation (7) may now be written as

$$\tilde{\psi}(x_1, x_2; \eta) = \int_A dq \tilde{\xi}(q, -q; \eta) \exp\left(-i2\pi q \frac{x_1 - x_2}{\Lambda}\right), \quad (8)$$

where $q = \frac{q_s \Lambda}{2\pi}$, with limits of integration A that depend on η and p as follows

$$q = \begin{cases} (1-\eta)(1-p) \rightarrow \eta(1+p) \& -\eta(1+p) \rightarrow -(1-\eta)(1-p), & \text{for } \eta < \frac{1}{2} \\ \eta(1-p) \rightarrow (1-\eta)(1+p) \& -(1-\eta)(1+p) \rightarrow -\eta(1-p), & \text{for } \eta > \frac{1}{2}. \end{cases} \quad (9)$$

The range of η is $(1-p)/2 < \eta < (1+p)/2$ if $p < \rho$ and $(1-\rho)/2 < \eta < (1+\rho)/2$ if $p > \rho$. The kernel of the integration in (8) is given by

$$\tilde{\xi}(q, -q; \eta) = \ell \text{sinc}\left(\frac{\ell}{\lambda_p} \left[n(\omega_p) - \sqrt{\eta^2 n^2(\omega_s) - (q\theta/2)^2} - \sqrt{(1-\eta)^2 n^2(\omega_p - \omega_s) - (q\theta/2)^2} \right]\right). \quad (10)$$

It is interesting to note the mixture of normalized bandwidth and slit width in determining the period of integration. This is a direct result of the high correlation between directions and frequencies in SPDC. Both the size of the physical apertures and the spectral bandwidth of the optical system determine the effective aperture of the system. Using equations (8)–(10) we can calculate the coincidence rate at the output plane as a function of the normalized separation $(x_1 - x_2)/\Lambda$ for the crystal orientations and thicknesses illustrated in the tuning curves of the previous section.

The coincidence rate $C(x_1, x_2)$ may now be calculated by substitution of (8) into (1). Let us start with the case of $\varphi = 36.44^\circ$ and $\ell = 0.1$ mm. Taking $\rho = 0.05$, $\theta = 0.03$ rad, and $p = 0.1$, we obtain the result in figure 3. This is a coincidence pattern (fourth-order coherence function) similar to the intensity interference pattern (second-order coherence function) that would be obtained by a coherent classical source of light. Referring to the corresponding tuning curve, we notice that these parameters correspond to downconverted light from the centre of the tuning curve, i.e. where the peak of the sinc function lies, and is essentially constant. The main factor determining the coincidence pattern would be the optical system, leading to the results shown. We obtain

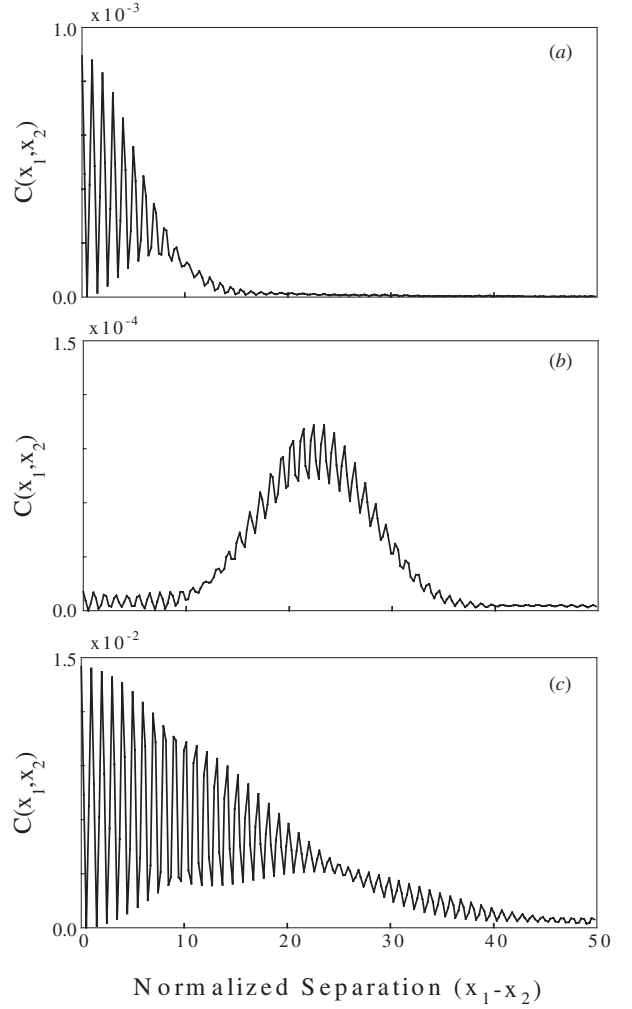


Figure 4. Coincidence rate as a function of normalized separation for $\varphi = 36.50^\circ$, $\ell = 10$ mm, $p = 0.1$, (a) $\theta = 0.03$, $\rho = 0.05$, (b) $\theta = 0.07$, $\rho = 0.05$, and (c) $\theta = 0.07$, $\rho = 0.1$.

similar results for the two other orientations of the crystal if all other parameters are held fixed, since for such a thin crystal the tuning curves exhibit enough uncertainty so as to render the three orientations almost the same over a wide range of frequencies and directions (centred around the direction of the pump wavevector).

As the thickness of the crystal increases, care must be exercised in choosing the parameters of the set-up. We shall take the case of $\varphi = 36.50^\circ$. For our given choice of bandwidth we must be careful in our choice of double-slit separation. If we choose an angle θ (angle subtended by the slits at the crystal, in this case 0.03 rad) that does intersect with the peak ridge of the sinc function, we shall obtain a coincidence pattern, shown in figure 4(a), that is similar to that previously obtained in figure 3. If, however, we increase the double-slit separation to 0.07 rad we shall obtain a coincidence pattern that is centred on a value other than zero (figure 4(b)). This is attributed to the occurrence of the interference between the sidelobes of the sinc function in the tuning curves. These sidelobes are modulated with a rate which depends on the crystal thickness. The new interference pattern is centred on a point proportional to the modulation frequency and thus the crystal length. The zero-

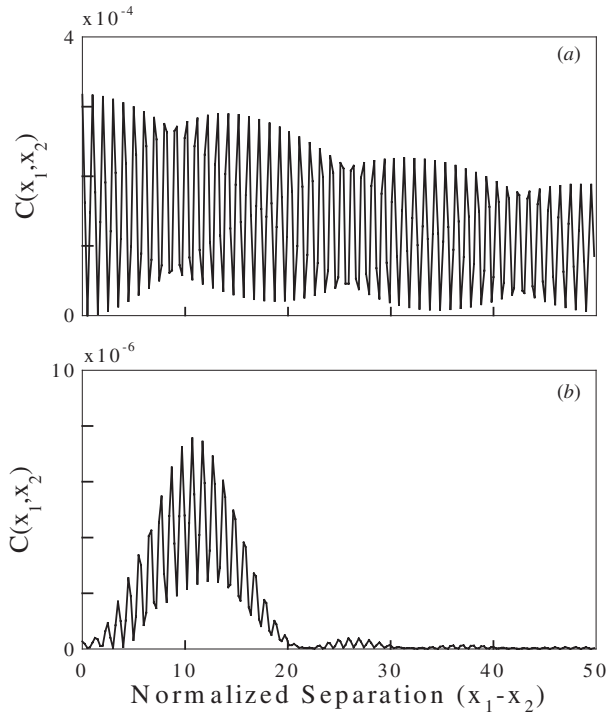


Figure 5. Coincidence rate as a function of normalized separation for $\varphi = 36.30^\circ$, $\ell = 10$ mm, $\theta = 0.05$, (a) $\rho = 0.2$, and (b) $\rho = 0.02$.

centred interference pattern can be restored by increasing the normalized bandwidth of the system to 0.1, i.e. by accepting a wider range of frequencies at the detectors (figure 4(c)). In this case the double-slits will intersect the sinc function at its peak and the effect of the sidelobes will diminish.

We next examine the case of $\varphi = 36.30^\circ$. In this case for a wide normalized bandwidth of 0.2 and an angle θ of 0.05 we obtain the coincidence pattern in figure 5(a). Decreasing the bandwidth while keeping the same double-slit separation will increase the contribution of the sidelobes to the interference as seen in figure 5(b) when the normalized bandwidth is decreased to 0.02.

5. Conclusions

We have studied the coincidence pattern formed behind a double slit when both signal and idler beams resulting from SPDC are transmitted through it. The coincidence pattern is sensitive to several parameters. The obtained coincidence pattern is analogous to the second-order interference pattern of a classical partially coherent source as long as the slits intersect the directions of the peak of the tuning curve in the

particular SPDC process. If this is not the case, and the double slit intersects the sidelobes of the tuning curve, a coincidence pattern is obtained but is shifted from the centre of the previous pattern and exhibits a different fringe width. Changing the crystal thickness, system bandwidth, or the direction of the crystal optical axis permits us to go from one case to the other with a fixed double-slit separation. Such a system therefore exhibits more degrees of freedom than its classical counterpart.

These results can be explained in another fashion. The double slit can be viewed as ‘sampling’ the fourth-order coherence function of the SPDC process in the NLC. This coherence function has a striking property: directions are strongly correlated to frequencies in accordance with the tuning curves of the parametric process. There is no classical counterpart to this behaviour.

It is clear that the double-slit interference experiment continues to yield valuable insights into the properties of light.

Acknowledgment

This work was supported by the U.S. National Science Foundation.

References

- [1] Saleh B E A and Teich M C 1991 *Fundamentals of Photonics* (New York: Wiley) chapter 10
Mandel L and Wolf E 1995 *Optical Coherence and Quantum Optics* (Cambridge: New York)
Born M and Wolf E 1999 *Principles of Optics* (Cambridge: Cambridge University Press)
- [2] Ribeiro P H S, Pádua S, Machado da Silva J C and Barbosa G A 1994 Controlling the degree of visibility of Young’s fringes with photon coincidence measurements *Phys. Rev. A* **49** 4176–9
Řeháček J and Peřina J 1996 Two-slit experiment with downconverted beams *Opt. Commun.* **125** 82–9
Stekalov D V, Sergienko A V, Klyshko D N and Shih Y H 1995 Observation of two-photon ‘ghost’ interference and diffraction *Phys. Rev. Lett.* **74** 3600–3
- [3] Fonseca E J S, Monken C H and Pádua S 1999 Measurement of the de Broglie wavelength of a multiphoton wave packet *Phys. Rev. Lett.* **82** 2868–71
- [4] Hong C K and Noh T G 1998 Two-photon double-slit interference experiment *J. Opt. Soc. Am. B* **15** 1192–7
- [5] Abouraddy A F, Nasr M B, Saleh B E A, Sergienko A V and Teich M C Demonstration of the complementarity of entanglement and coherence in the spatial domain at press
- [6] Saleh B E A, Abouraddy A F, Sergienko A V and Teich M C 2000 Duality between partial coherence and partial entanglement *Phys. Rev. A* **62** 043816
- [7] Malugin A A, Penin A N and Sergienko A V 1981 Efficient generator of a two-photon field of visible radiation *Sov. J. Quantum Electron.* **11** 939–41